Wind Profile Estimation from Aircraft Derived Data Using Kalman Filters and Gaussian Process Regression

Sun, J.; Marinescu, M.; Olivares, Alberto ; Staffetti, Ernesto

Publication date
2021

Document Version
Final published version

Citation (APA)
Sun, J., Marinescu, M., Olivares, A., & Staffetti, E. (2021). *Wind Profile Estimation from Aircraft Derived Data Using Kalman Filters and Gaussian Process Regression*. Paper presented at 14th USA/Europe Air Traffic Management Seminar.

Fourteenth USA/Europe Air Traffic Management Research and Development Seminar (ATM2021)

Wind Profile Estimation from Aircraft Derived Data Using Kalman Filters and Gaussian Process Regression

Marius Marinescu, Alberto Olivares, Ernesto Staffetti
School of Telecommunication Engineering
Rey Juan Carlos University
Fuenlabrada, Madrid, Spain
marius.marinescu@urjc.es,
alberto.olivares@urjc.es, ernesto.staffetti@urjc.es

Junzi Sun
Faculty of Aerospace Engineering
Delft University of Technology
Delft, The Netherlands
j.sun-1@tudelft.nl

***Abstract*—Accurate wind information is crucial in air traffic management, for instance, to improve trajectory predictability and precision in controlled time of arrival. Nowadays, air traffic management relies on Numerical Weather Prediction, which usually has a low resolution and low update rate. A potential approach for improving the resolution and accuracy of the weather predictions consist in using airborne aircraft as meteorological sensors. Aircraft surveillance systems such as ADS-B and Mode S, transmit data related to weather conditions, automatically or in response to interrogation by air traffic control surveillance radars. In this paper, three different methods for constructing wind profiles from surveillance data have been applied and a comparison between them carried out. The first two methods being modifications of the Kalman filter have been referred to as the Adapted Kalman Filter and Smooth Adapted Kalman Filter. The third one is based on Gaussian process regression. The Kalman filter based methods are able to assimilate nearby data in a straightforward way and update the wind speed estimation in real time. Gaussian process regression is a very flexible and general regression model that can smoothly interpolate in space and extrapolate in time. These three methods have been validated using a test data set, achieving a 50% reduction of the prediction uncertainty in comparison with a baseline model. In addition, the Gaussian process methodology has been applied to reconstruct and forecast the wind field.**

***Keywords*—Wind Estimation; Kalman Filter; Gaussian Process Regression; Air Traffic Management; ADS-B; Mode S.**

I. Introduction

Improving capacity, efficiency, safety, and reducing costs and environmental impact of Air Traffic Management (ATM) system are the main objectives of the Single European Sky ATM Research (SESAR) and the Next Generation Air Transportation System (NextGen) projects, among others. Both projects are based on the concept of Trajectory-Based Operations (TBO). The idea behind TBO is to enable the ATM system to know and, when appropriate, modify the aircrafts planned and actual trajectories, before or during flight, based on accurate information shared among stakeholders. The enabling technology is the System-Wide Information Management[1] (SWIM) project, a European system not yet fully deployed with the goal of achieving a full integration of flight information in order to create a synchronised view of flight data by all actors.

In the TBO framework an important aspect is trajectory predictability, which can be improved by planning aircraft trajectories using quality weather information. In particular, this requires precise wind information [1], [2].

Nowadays, aircraft trajectory planning relies on winds reports from Numerical Weather Prediction (NWP) models. NWP observations are mainly gathered from radiosondes and aircraft equipped with Aircraft Meteorological Data Relay (AMDAR). However, the NWP meteorological information generally has a coarse grid resolution and an update rate at most once an hour such as National Oceanic and Atmospheric Administration (NOAA) Rapid Refresh[2]. In Europe, Aeolus satellite data is beginning to be used [3]. The European Centre for Medium-Range Weather Forecasts (ECMWF) has been including Aeolus data in its forecasts since January 2020, and they have been distributed publicly to forecasting services and scientific users with a time delay of three hours since July 2020. The satellite can deliver vertical profiles that show the horizontal speed of the world's winds in the lowermost 26 km of the atmosphere. Moreover, radiosondes are launched at specific times, no more than four times per day, the spatial distribution of which is too coarse. In addition, most of the aircraft are not equipped with the AMDAR system. Due to these limitations, current weather predictions are unlikely to satisfy the future ATM system requirements [4]. These limitations can be resolved using meteorological aircraft derived data, in which aircraft are employed as airborne meteorological sensors. With this aim in mind, the Royal Netherlands Meteorological Institute (KNMI) has established the so called European Meteorological Aircraft Derived Data Center (EMADDC). One of the activities of this centre is to distribute derived wind and temperature data. Mode S data began to be available to users in July 2020[3]. A methodology based on Mode S data has the advantage of a high grid resolution and on-demand refresh rate [5]. Mode S observations are gathered every few seconds. According to Flightradar24[4], there are normally more than 10,000 aircraft

[1] https://www.eurocontrol.int/concept/system-wide-information-management

[2] https://rapidrefresh.noaa.gov

[3] https://www.ecmwf.int/en/newsletter/164/news/emaddc-mode-s-new-source-aircraft-data-over-europe

[4] https://www.flightradar24.com

in the air around the world at any one time - and this figure is set to increase.

When estimating the wind using aircraft derived data, three important features must be taken into account: the estimation resolution, update rate, and confidence level of prediction. This can be achieved using data assimilation techniques as those implemented in this paper. The main contributions of this work are the following: firstly, a Gaussian Process Regression (GPR) has been considered for estimating wind profiles. In this paper, an iterative version of GPR has been implemented, which enables nowcasting. To the best of the authors' knowledge, GPR models have not been used in this context. Second, a variant of the Kalman Filter (KF) proposed in [6] has been employed. In this variant, the transition matrix is no longer the identity matrix and has been designed to model the spatio-temporal relation among elements of the state vectors in the prediction step. This approach provides smoother wind profiles than the original KF, in accordance with the fact that wind speed is a continuous variable. Finally, an evaluation of the performance of these methods and a comparison have been carried out. The obtained results show that GPR achieves the best performance.

This paper is structured as follows. Section II provides background information regarding data treatment and wind estimation. Section III describes the mathematical development of the wind estimation methods and in Section IV, the setup of the case study and parameters. The performance of the proposed techniques is tested in Section V and in Section VI, reconstruction and forecast of wind field is discussed. Finally, conclusions are drawn in Section VII.

II. Background

This section discusses the data features, the procedure via which information is derived from data, the current methods for wind estimation, and the case study.

A. ADS-B and Mode S

Automatic Dependent Surveillance-Broadcast (ADS-B) is a surveillance technology that enables the automatic broadcast of aircraft flight states. ADS-B relies primarily on global navigation systems to obtain the flight states of position and ground speed, which are transmitted periodically at a rate of every 0.5 seconds, approximately.

The most common implementation of ADS-B is through the Mode S extended squitter. Mode S is a selective interrogation protocol employed by air traffic controllers to obtain additional flight states other than the position and altitude. Within Mode S Enhanced Surveillance communication protocol, a set of parameters related to aircraft airspeed are interrogated by surveillance radar and transmitted by aircraft.

Mode S signals, including ADS-B signals, can be freely received by researchers around the world. The inference and decode of these signals can also by achieved using open source tools like pyModeS [7]. The ground speed, track angle, airspeed, and heading are used to generate the wind observations.

B. Wind Estimation

In order to estimate the wind, the true airspeed needs to be calculated first, based on the Mach number and indicated airspeed that are transmitted by the aircraft in Mode S communication. This is performed using aeronautical airspeed conversions under International Standard Atmosphere (ISA) conditions.

Once the true airspeed, ground speed, heading, and track angles are known, the wind vector can be calculated as the difference between ground speed vector and true airspeed vector. Fig. 1 illustrates the relationship among these vectors. Here, χ_g, χ_a, and χ_w represent the ground track, heading, and wind direction, while V_{gs}, V_{tas}, and V_w represent the ground speed, true airspeed, and wind speed vectors, respectively.

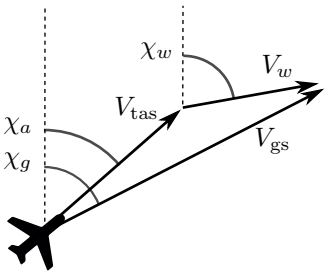

Figure 1. Relationship between true airspeed, ground speed, and wind vectors.

C. Current Methods for Wind Estimation

Different approaches have been employed during the last decades to take advantage of the surveillance data in the meteorological framework. In [8] and [9], it has been shown that assimilation of weather surveillance has a positive impact on Regional NWP models. Kriging, a geostatistical method, is used in [10] to generate short-term weather prediction along trajectories. An innovative model combining particle filtering and Lagrangian transportation modeling is employed for weather field reconstruction in [11]. Aircraft wind observations have been used in [2] to update the optimal descent trajectory in real-time. In [12], statistical data and Kalman filtering have been used to predict wind for trajectory predictions. In [13] and [14], Kalman filtering has been used in wind field estimation to reduce measurement noise. It has also been recently used to estimate wind in aircraft turns with a high roll angle [15]. Lastly, Kalman filtering has been used in [6] to create an aircraft moving wind profile for continuous descent operations and spacing performance.

D. Wind Profile and Case Study

The wind profile is a vertical representation of the horizontal mean wind speed. In analogy with the ISA model for temperature, there are empirical functions describing this profile. The best known are: the log wind profile, which describes a standard wind in the planetary boundary layer under stable atmospheric conditions; and the power law wind profile, which relates the wind speed at one altitude to those at other altitudes [16]. In the case study presented in this paper, a precise estimation of the wind profile at two

different positions is performed. More precisely, the RILKO Initial Approach Fix (IAF) and the Final Approach Fix (FAF) neighbouring the airport Adolfo Suarez Madrid-Barajas have been chosen. The former has coordinates $40°58'44.1''N$, $3°47'48.6''W$ and the latter has coordinates $40°40'59.4''N$, $3°34'32.6''W$, as shown in the navigation chart[5] represented in Fig. 2. Data collected at the RILKO IAF describe the wind profile at altitudes around 3.3 km, while the FAF has been chosen to study the wind profile at lower altitudes of around 1.2 km. The FAF also allows the number of test points to be duplicated, since all aircraft passing through the RILKO IAF also pass through the FAF. The position of the wind profiles along with a landing aircraft path can be observed in Fig. 3.

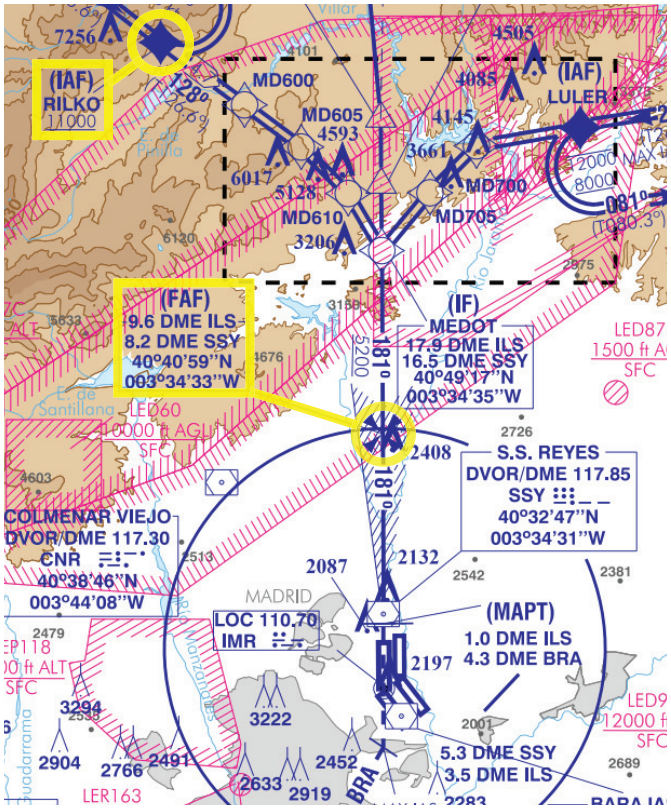

Figure 2. Instrument approach chart IAC/6 LOC RWY 18R. Source Spanish AIP service. Not for operational use.

III. Wind Profile Estimation Methods

This section describes wind speed estimation using the Adapted Kalman Filter (AKF) first and goes on to present the Smooth Adapted Kalman Filter (SAKF). These two methods are based on the classic linear Kalman filter [17], which has been used in [18] for meteorological data assimilation. Finally, the method employed for wind estimation using GPR is introduced.

A. Adapted Kalman Filter

The AKF is a variant of the Airborne Wind Estimation Algorithm (AWEA) proposed in [6], which is an adaptation

[5] The full navigation chart can be consulted in the webpage of the Spanish AIP service https://aip.enaire.es/AIP

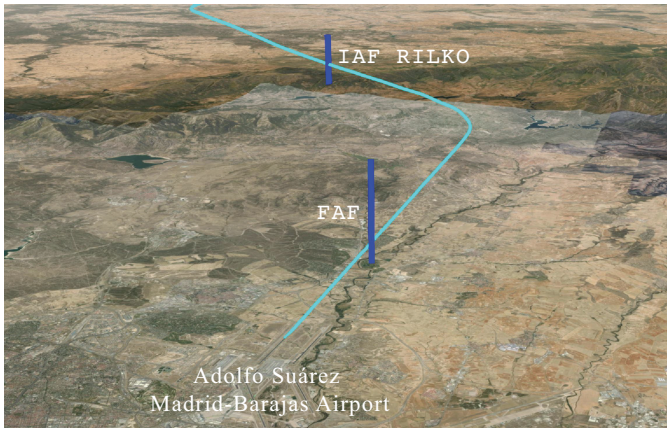

Figure 3. The cyan trajectory represents an approach aircraft path. Blue vertical lines represent the locations where wind profiles are estimated.

of the classic KF. The key idea in the AWEA is to modify the appropriate covariance matrix to take into account the uncertainty of the observations. Specifically, the covariance matrix considers physical distances between the wind observations and the points where the wind is to be estimated.

Generally, the KF consists of two stochastic equations:

$$\mathbf{x}_k = M_k\mathbf{x}_{k-1} + \mathbf{w}_k \quad \text{(state equation)} \tag{1a}$$

$$\mathbf{y}_k = H_k\mathbf{x}_k + \mathbf{v}_k \quad \text{(measurement equation)} \tag{1b}$$

The state equation 1a models the dynamics of the system including unobserved or hidden states. It describes the evolution of state in time. The measurement equation 1b models the observed variables and describes the relationship between the observation and true states of the variables.

In the state equation 1a, $\mathbf{x}_k$ is the wind speed vector at time k, M_k the transition matrix, and $\mathbf{w}_k$ the process noise. In the measurement equation 1b, $\mathbf{y}_k$ is a vector containing the measured wind speeds at time k, H_k is the observation matrix defining the relationship between state variables and observations, and finally $\mathbf{v}_k$ is the measurement noise. It is worth noting that matrices M_k and H_k indicate linear relationships between variables. This is a simplified form of the general model, where, instead of matrices, M_k and H_k are replaced by nonlinear operators.

The matrix M_k in the KF allows modeling of the dynamics of the hidden state $\mathbf{x}_k$, which in our case, represent the wind profile. As in AWEA wind dynamics are not considered in the AKF method, therefore M_k is reduced to the identity matrix $I_{n\times n}$, where n is the number of altitude intervals. The model errors $\mathbf{w}_k$ and $\mathbf{v}_k$ are assumed to be unbiased, uncorrelated, and with covariance matrices:

$$Q_k = \mathbb{E}[\mathbf{w}_k\mathbf{w}_k^t] \tag{2}$$

$$R_k = \mathbb{E}[\mathbf{v}_k\mathbf{v}_k^t] \tag{3}$$

At each time step t_k, the KF algorithm is as follows:

1) At $k = 0$ the algorithm is initialized. An initial wind speed vector is given as $\mathbf{x}_0^{\mathrm{f}}$, where the superscript f indicates forecast. An error covariance matrix of this estimation, P_0^{f}, is also given as an input.

2) If $k \geq 1$:
   a) Analysis
      - The Kalman gain matrix is computed with the formula: $K_k = P_k^{\mathrm{f}} H_k^t (H_k P_k^{\mathrm{f}} H_k^t + R_k)^{-1}$. This matrix is based on the uncertainties in the current state and the new measurements.
      - The state vector is updated using the new observations with the formula: $\mathbf{x}_k^{\mathrm{a}} = \mathbf{x}_k^{\mathrm{f}} + K_k(\mathbf{y_k} - H_k \mathbf{x}_k^{\mathrm{f}})$, where the superscript a stands for analysis.
      - The covariance matrix of the analysis estimation is computed as: $P_k^{\mathrm{a}} = (I - K_k H_k) P_k^{\mathrm{f}}$.
   b) Forecast
      - The forecast of states for the next time step is calculated as: $\mathbf{x}_k^{\mathrm{f}} = M_{k+1} \mathbf{x}_k^{\mathrm{a}}$.
      - The error covariance matrix of this estimation is calculated as: $P_k^{\mathrm{f}} = M_{k+1} P_k^{\mathrm{a}} M_{k+1}^t + Q_{k+1}$.

In this paper, the algorithm is used to compute the wind speed profile. The matrices $M_k = I$ and $Q_k = Q$ are assumed constant. The R_k matrix, which models the measurement errors, is updated at each time step, taking into account the uncertainty of the observations. If m observations are available at time interval $[t_k, t_{k+1})$, the R_k matrix becomes:

$$R_k = \begin{pmatrix} \sigma_1^2 & 0 & 0 & \cdots & 0 \\ 0 & \sigma_2^2 & 0 & \cdots & 0 \\ \vdots & \vdots & \vdots & \ddots & \vdots \\ 0 & 0 & 0 & \cdots & \sigma_m^2 \end{pmatrix}_{m \times m} \tag{4}$$

$$\sigma_i^2 = \left[1 + \alpha \frac{d(i)}{215} \right] \cdot \sigma^2 \tag{5}$$

where σ is the instrumental measurement error, $d(i)$ is the great circle distance from the observation to the waypoint in NM, and α is a scaling parameter. In this way, the measurement error is modelled as a function of the distance. For example, if the observation is at 215 NM away and α is chosen to be one, the error becomes $(1+1)\sigma^2 = 2\sigma^2$, which is twice the typical instrumental error σ^2.

The H matrix is computed such that the observations are linearly interpolated in the altitude grid. For example, considering an observation i at $11,700$ ft, the closest discretized altitudes levels are at 11,500 ft and 12,000 ft. The i-th row in the matrix H that corresponds to this observation is computed as:

$$H_{i \times 1:n} = \begin{pmatrix} 0 & 0 & 0 & \cdots & 0.6 & 0.4 & \cdots & 0 \end{pmatrix}_{1 \times n}, \tag{6}$$

where n indicates the number of altitude intervals, which depends on the chosen resolution.

B. Smooth Adapted Kalman Filter

The SAKF method is similar to the AKF. The idea is to construct a smoother filter, as wind speed is a continuous variable. As shown in Section IV, the AKF usually generates peaks at the discretization points and the resulting wind profile has a saw shape. To achieve a smooth estimation, the state matrix M_k in the SAKF is adjusted so that it is no longer a simple identity matrix. The idea is to assign weights to the values of the state vector $\mathbf{x}_k = (x_k^1, x_k^2, ..., x_k^n)^t$ in order to make each element x_k^j dependent on the neighborhood points x_k^{j-1} and x_k^{j+1}. Thus, the following matrix is proposed:

$$M_k = \begin{pmatrix} \alpha_1 & \alpha_2 & 0 & 0 & \cdots & 0 & 0 \\ \alpha_2/2 & \alpha_1 & \alpha_2/2 & 0 & \cdots & 0 & 0 \\ 0 & \alpha_2/2 & \alpha_1 & \alpha_2/2 & \cdots & 0 & 0 \\ \vdots & \vdots & \vdots & \vdots & \ddots & \vdots & \vdots \\ 0 & 0 & 0 & 0 & \cdots & \alpha_2 & \alpha_1 \end{pmatrix}_{m \times m}, \tag{7}$$

with weights $\alpha_1, \alpha_2 \in [0, 1]$, $\alpha_1 + \alpha_2 = 1$. In this way, an updated estimation at point x_k^j is built as the combination of α_1 the estimation at that point, and α_2 the estimation at the neighborhood points.

C. Gaussian Process Regression

GPR has applications in a wide variety of disciplines, such as finance, physics, geostatistics or machine learning [19], [20].

A Gaussian Process (GP) is a stochastic process $\{Z_a\}_{a \in S}$, where S is the index set, in which any sample of the process $Z_{a_1}, Z_{a_2}, ..., Z_{a_k}$ is jointly Gaussian distributed for all k, and all choices of $a_1, ..., a_k$. This definition applies to both discrete and continuous time random processes. GP models are very flexible in the sense they are suitable for data patterns with different properties, such as linearity, periodicity, symmetry, continuity, differentiability, or non differentiability. In Fig. 4, these different patterns represented as wind profiles are illustrated.

A GPR model addresses the question of predicting the value of a variable y given the predictor variables $\mathbf{x}$. In this case, y is the wind speed and $\mathbf{x} = (t, x, y, z)^t$ corresponds to time and position. Given a linear regression model of the form

$$y = \mathbf{x}^t \beta + \varepsilon, \quad \varepsilon \sim N(0, \sigma^2), \tag{8}$$

where parameters β and error variance σ^2 are estimated from the data, the GPR model predicts the variable y by introducing two new features:

- A latent random variable $f(\mathbf{x})$ from a Gaussian process. For any sample of points, $f(\mathbf{x}_1), f(\mathbf{x}_2), f(\mathbf{x}_3), ..., f(\mathbf{x}_n)$ are jointly Gaussian distributed with zero-mean and covariance function $k(\mathbf{x}, \mathbf{x}^t)$. The covariance is used to model properties and smoothness of the response variable y.
- A basis function h that projects the inputs $\mathbf{x}$ into a $p-$dimensional feature space.

Combining these definitions, the GPR model can be expressed as:

$$y = h(\mathbf{x})^t_{1 \times p} \beta_{p \times 1} + f(\mathbf{x}) + \varepsilon. \tag{9}$$

It has been shown in [20] that under these assumptions the response variable y is also Gaussian distributed. For a fixed point $\mathbf{x}_i$ and a known realization $f(\mathbf{x}_i)$ of the Gaussian process at the point, it follows that:

$$y \sim N(h(\mathbf{x}_i)^t \beta + f(\mathbf{x}_i),\ \sigma^2). \tag{10}$$

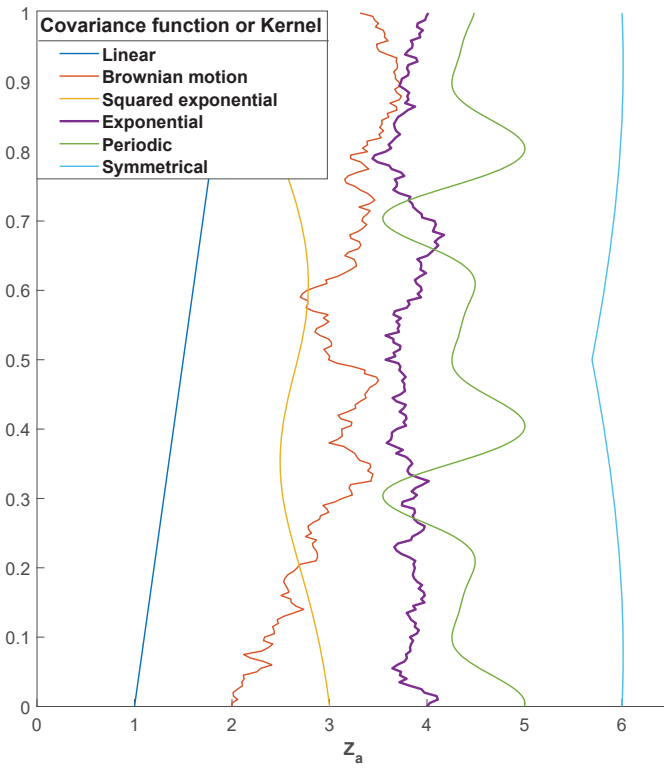

Figure 4. Realizations of different Gaussian processes, generated by diverse covariance matrices or kernel.

This feature makes GPR an effective tool, since it is able to give not only an estimation but also the distribution of the estimates. This allows, for example, a confidence interval for the estimators to be provided.

IV. Implementation

In this section the data set and the implementation details are discussed. For the simulations, All-Purpose Structured EUROCONTROL Surveillance Information Exchange (ASTERIX) aircraft data, courtesy of the Spanish National Air Navigation Service Provider, in the vicinity of Madrid Adolfo Suarez Madrid-Barajas airport have been used. Wind speed is calculated using the methods described in Section II-B.

In order to have a more accurate wind observation, noisy data and outliers must be removed. It is well known that wind data collected during roll manoeuvres are less reliable [5]. In Fig. 5, aircraft roll angle and wind speed have been represented versus time. It can be seen that noise in wind speed increases when the aircraft has a high roll angle. Therefore, data collected with roll angle larger than 5° have been removed. After the removal of low-quality data, outliers were considered. Data have been grouped in based on the altitude. Sets having a vertical extent of 1 km have been considered. In each group, the usual interquartile range method for outlier removal has been applied. They correspond to outliers commonly seen in a boxplot.

In all models, the instrumental error used was $\sigma = 3$ m/s, which is a typical wind measurement error [6]. In the AKF

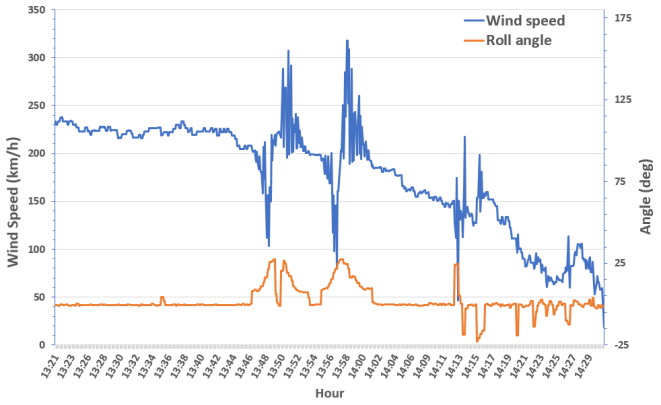

Figure 5. Roll angle and wind speed versus time.

and SAKF models, the initial wind speed has been estimated based on a standard logarithmic wind profile according to the power-law described in [16]. The starting matrices are $Q_0 = I$, $R_0 = \sigma^2 \cdot I$, and $P_0 = \sigma^4 I$. The chosen elements of the diagonal matrix P_0, are large to give uncertainty to the initial estimation. This allows the filter to adapt quickly to new incoming data. For the SAKF model, α_1 and α_2 have been set to 0.6 and 0.4, respectively.

In the GPR framework, the following parameters must be estimated: the coefficients of the basis function β, the instrumental variance σ^2, which has been assumed fixed, and the hyperparameters θ, if a parametric kernel function is chosen to define the covariance matrix. In this paper, the exponential kernel is chosen [20]:

$$k(\mathbf{x}_i, \mathbf{x}_j/\theta) = \sigma_f^2 e^{-r}, \tag{11}$$

where

$$r = \sqrt{\sum_{m=1}^{d=4} \frac{(x_{im} - x_{jm})^2}{\sigma_m^2}}. \tag{12}$$

With this kernel, the correlation between two points decreases exponentially as a function of the Euclidean distance in space and time. Before computing the distance, each input variable x_{im} has been scaled by a factor σ_m^2, which takes into account the different scales of the input variables. This is very important since in this case the variables are anisotropic, i.e., not homogeneous [10]. The correlation scale in position is different from the correlation scale in time. In other words, the scaling factors define how far apart the input values $\mathbf{x}_i$ must be so that the response values can be considered uncorrelated. Usually, σ_m is called the characteristic length scale. Having time and space variables as input, GPR allows estimations and predictions to be performed, i.e., to interpolate in space and to extrapolate in time, respectively.

Finally, the chosen basis function h was:

$$h(\mathbf{x}_i) = \begin{pmatrix} 1 & \mathbf{x}_i^t \end{pmatrix}_{5\times 1}^t. \tag{13}$$

In this way the mean of the process changes linearly with respect to the input variables.

V. Performance Evaluation

The models are trained and tested with a 2-hour and 5-minute data set. Fig. 6 shows, all the aircraft paths contained in the data set.

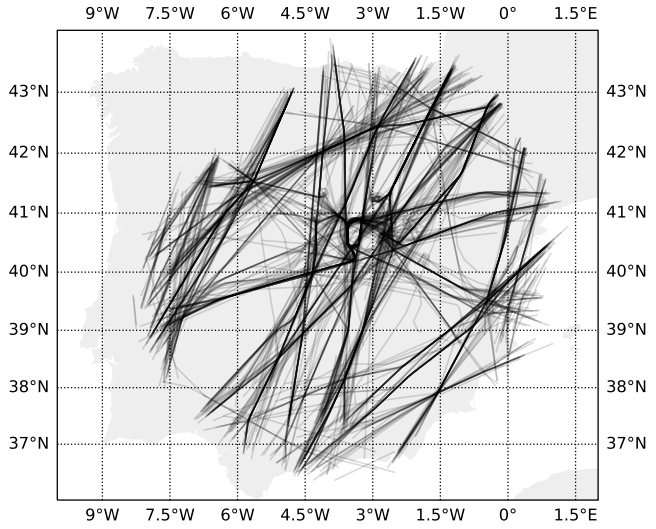

Figure 6. Aircraft paths contained in the data set.

In the case of the GPR model, only the data in a square region with a size of 240 by 240 km centered on the Adolfo Suárez Madrid-Barajas airport are considered. In Fig. 7, the training and test data is illustrated. The test paths are those which pass through the waypoints RILKO IAF and FAF, represented as dots.

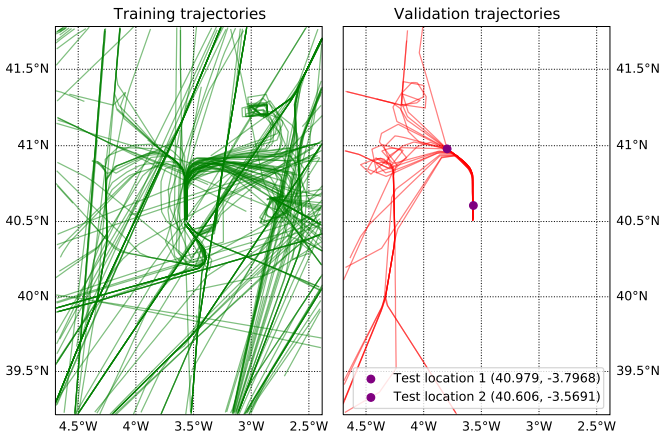

Figure 7. On the left, training trajectories around the Adolfo Suárez Madrid-Barajas airport. On the right, the trajectories used for testing.

The time discretization or refresh rate of the estimators is 0.5 minutes and the altitude discretization is 500 ft, ranging from 2,000 ft to 20,000 ft.

A simple wind profile, referred to as the baseline model, has been computed for comparison of the performance between the AKF, SAKF, and GPR methods. This baseline model is initiated with the same wind profile as in the AKF and SAKF methods. Subsequently, each time step the estimation is updated at each altitude by computing the mean of the available data. If no data is available at the respective altitude interval, the corresponding estimation remains unchanged. This baseline model will give an idea of how much performance our models achieve in comparison to merely averaging the available data.

The chosen data correspond to a windy day on December 21, 2019. The maximum wind speed reaches 100 m/s (360 km/h). The general scheme for estimation and validation is as follows:

1) The AKF, SAKF, and baseline estimators initiate at 13:45, 15 minutes before validation. This acts as a burn-in period.
2) A first GPR model is trained with one-hour data from 12:55 to 13:55. The training is performed by selecting a subset of 2,000 data points, allowing the GPR to be ready in less than 5 minutes. For prediction, the *Block Coordinate Descent Approximation* method has been used which allows for a fast and accurate prediction [21].
3) The validation starts at 14:00 UTC. The wind speed profiles are compared with the testing data coming from the landing aircraft when passing through the considered points the RILKO IAF and the FAF. Every 15 minutes, a new GPR model is trained to detect possible trend changes in wind speed.
4) Validation finishes at 15:00, when the Root Mean Square Error (RMSE) and the Mean Absolute Error (MAE) of the estimated wind profile are computed using the test data.

Fig. 8 represents the wind profiles estimations along with the training and testing data at two different time instants. The contrast in smoothness between the AKF and SAKF can be clearly seen. The GPR also achieves a smooth estimation. This is because values close in time and space are correlated through the exponential covariance matrix (11).

Table I shows the RMSE and MAE for the different estimation approaches. As expected, the baseline model has lower performance in comparison with the other methods.

The SAKF method, despite giving smoother results than the AKF, as required for a continuous variable, does not improve its estimation. Indeed, for an estimator, not only smoothness but also the ability to produce unbiased estimations that reflect wind characteristics at each position in space is important. This is better achieved by the GPR where the estimation is unbiased (see Fig. 9). Furthermore, the GPR adapts better to wind characteristics at each position in space, since significant differences between the estimations at the RILKO IAF and the FAF waypoints can be observed. Nevertheless, in the case of the KF-based methods differences between wind profiles at the waypoints are low and are not always visible. They do not capture as well as GPR the behaviour of the wind at each point in space because the KF-based methods compute "weighted means" of the data. This advantage of GPR models is achieved by its principal characteristic, the covariance function, which allows the relationship between wind in space and time to be described. It can also be observed that GPR and KF estimations differ at the key altitudes of the RILKO

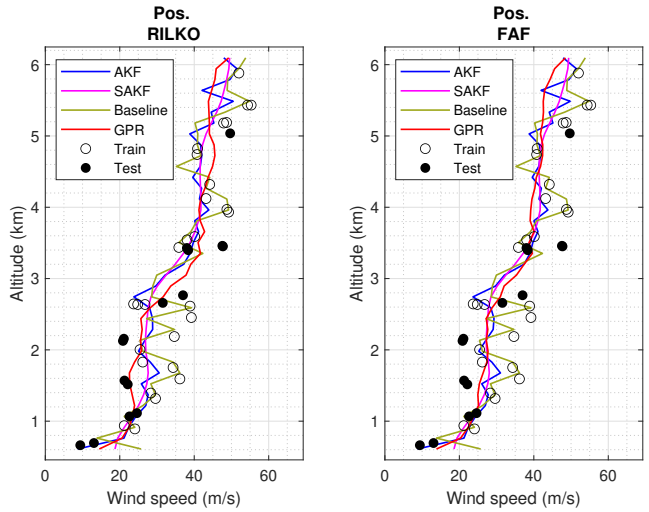

(a) Wind profiles at 14:30 along with training and testing data available at that time.

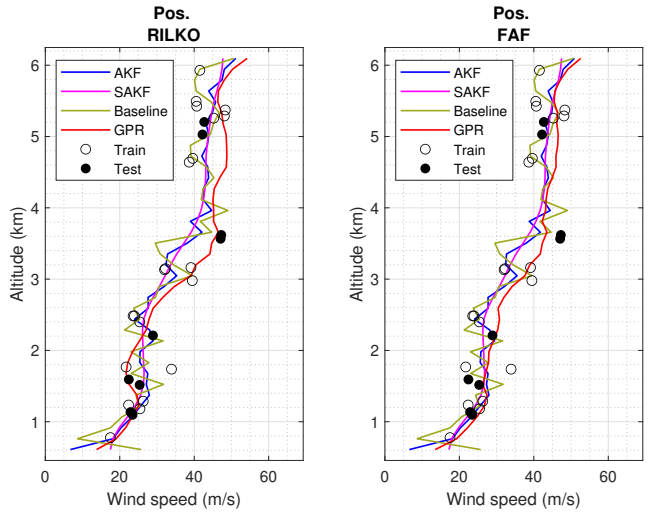

(b) Wind profiles at 14:45 along with training and testing data available at that time.

Figure 8. Estimated wind profiles based on different methods.

IAF, around 3.3 km or 11,000 ft, but lesser at the key altitude of the FAF, 1.2 km or 4,000 ft. This difference is due to KF benefits of spatially close wind speed information, since aircraft landing in the adjacent track, pass close to the FAF.

Type	AKF	SAKF	Baseline	GPR
RMSE (m/s)	4.3	4.8	5.9	3.0
MAE (m/s)	3.2	3.4	4.3	2.3

TABLE I. Wind speed errors when no landing aircraft wind measurements passing through the chosen waypoints are given to the models.

Fig. 9 shows the boxplot of the errors obtained for each method. In general, GPR has a lower spread, whereas with AKF and SAKF methods wind speed values are underestimated.

Since all data collected by aircraft passing through the chosen waypoints is only contained in the testing data set, the

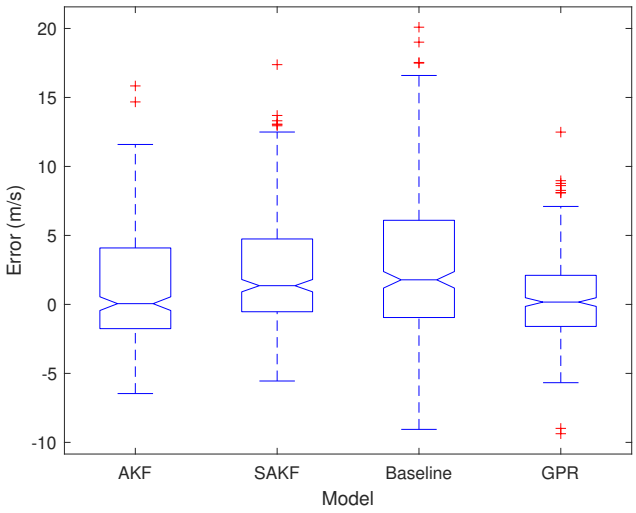

Figure 9. Test errors boxplot for the different methodologies.

showed results are worst case scenarios. If our testing data selection criteria is relaxed by including some of the flights passing these waypoints, the performances are expected to be increased. Table II show clearly how estimation errors improve when half and all of the testing data set are transferred to the training data set. We point out that no significant improvement can be observed using the GPR model. This indicates that the GPR model already has a good performance, and better performance is not got by including more data.

In contrast, KF-based methods benefit from more training data collected by aircraft passing through the waypoints.[6] By dispensing data that pass through the waypoints, KF methods produce higher weight on these observations, since the distances to waypoints are practically zero. Finally, the KF-based methods performance can be further improved if all flights passing these waypoints is provided, as can effectively be seen in Table II and the boxplots of Fig. 10.

Type	Transferred test	AKF	SAKF	Baseline	GPR
RMSE (m/s)	50%	3.6	4	5.3	3.1
MAE (m/s)	50%	2.6	3	3.8	2.4
RMSE (m/s)	100%	3.2	3.6	4.9	2.9
MAE (m/s)	100%	2.4	2.7	3.5	2.2

TABLE II. Wind speed errors when 50% and 100% of the testing data are given to the models.

VI. Estimation and Forecast of Wind in a Continuous Field

In earlier sections, the proposed GPR approach is used to generate 1D vertical wind profiles at specific locations. However, this approach can be extended to the entire 2D or 3D spaces.

[6] Generally, the KF is less capable of knowing the wind speed behavior at the waypoints, which may be different from the average behavior of the data.

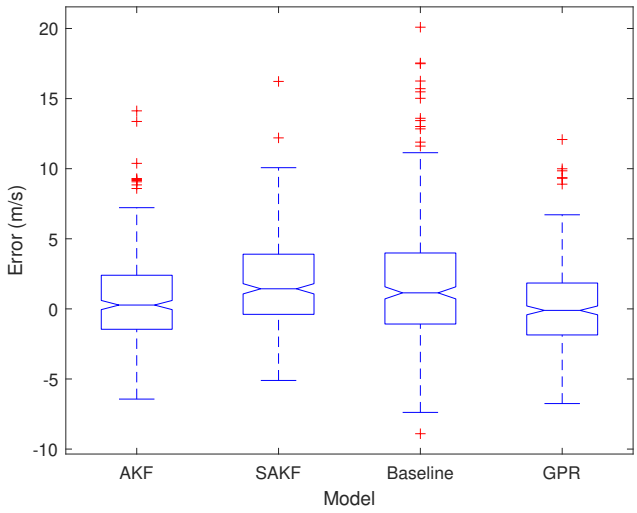

Figure 10. Test errors boxplot for the relaxed scenario where data passing through waypoints is dispensed.

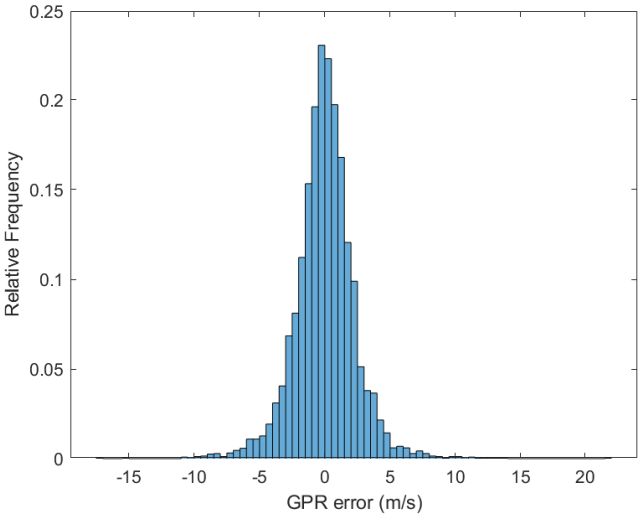

Figure 11. Wind field reconstruction error histogram.

In this section, we focus on applying the proposed GPR wind estimation method to all locations around the Terminal Manoeuvring Area (TMA). Both the reconstruction and forecast of wind fields are discussed. For better illustration, specific altitudes are selected for the demonstrations.

A. *Wind Field Reconstruction*

The objective is to reconstruct the wind speed field at a specified time. Concretely, the same implementation as in Section IV is performed with the following distinctions:

- Only the GPR method is used.
- The chosen kernel is the squared exponential, illustrated in Fig 4. The difference with respect to the kernel described in (11) is that r is now squared. This allows for a smoother estimation of the wind field.
- The focus is on wind field reconstruction instead of prediction. Now, the estimation is made all over a square region with a size of 240 by 240 km centered on the airport. To evaluate the performance of the reconstructed wind field, 20% randomly selected data points are reserved for testing.

In Table III the errors of the GPR models are shown. The errors represents about 4.5% of the real measurement. Taking into account the fact the data itself includes instrumental errors and wind speed ranges from 3 m/s to 100 m/s, the achieved performance is satisfactory. Fig. 11 displays the error histogram distribution. It can be observed that the errors are symmetrically distributed, non-biased and bell-shaped, as expected for a well-trained GPR model.

Type	GPR
RMSE (m/s)	2.3
MAE (m/s)	1.6
MAE (in percentage)	4.5%

TABLE III. Wind speed errors for the wind field reconstruction.

With the aim to illustrate the wind speed field, the reconstruction at a specific time instant and two different altitudes is shown in Fig. 12. In the plots, the z-axis represents wind speeds, while the x-axis and y-axis represent a region around the airport. Selected train and test points close in time and altitude are also depicted.

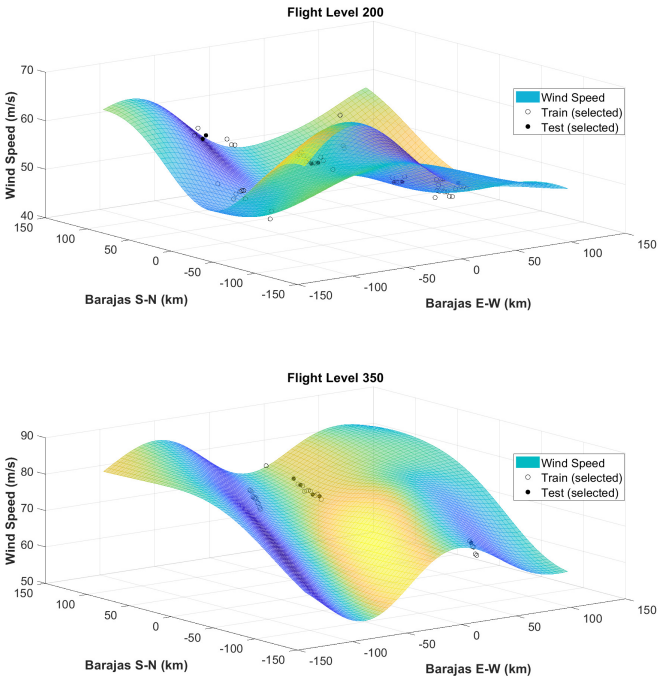

Figure 12. Wind field reconstruction at time 13:25 at two specific flight levels. Black dots refers to a selection of training and testing points close in time and altitude, ± 7.5 min and ± 500 ft.

B. *Wind Field Forecast*

This experiment aims to demonstrate the capability of GPR in predicting scalar wind field at close future time instants. The procedure is similar to the wind field reconstruction one,

except for the source of testing data. Instead of randomly choosing the data from 12:55 to 13:55, all future data points in a 15-minutes range, from 14:00 to 14:15, are considered for testing. This process is repeated every 15 minutes for one hour.

Fig. 13 shows, 15-minute predictions of the wind field at two different altitudes along with some selected test points.

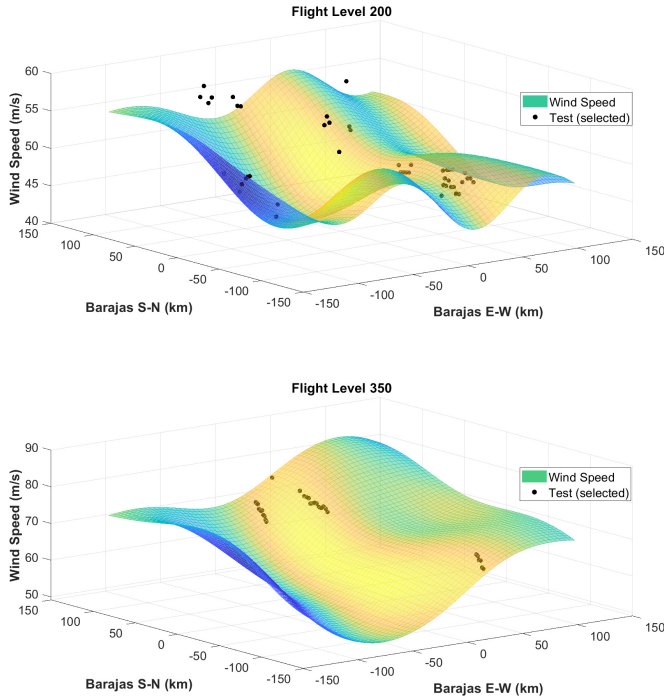

Figure 13. Wind field prediction at time 14:10 at two specific flight levels. The prediction is made for 15 minutes in the future with the model trained from 12:55 to 13:55. Black dots refers to a selection of testing points close in time and altitude, ± 7.5 min and ± 500 ft.

Based on all available data, the accuracy of the GPR wind prediction model with 15 minutes look-ahead time horizon can be analysed. Table IV shows a summary of the error statistics on RSME and MAE across all the process. It is noticeable that the accuracy of the wind forecast is lower than the reconstructed wind in Table III.

Type	GPR
RMSE (m/s)	5.9
MAE (m/s)	4.4
MAE (in percentage)	9.5%

TABLE IV. Wind speed errors for the wind field forecast.

Another way to evaluate the performance of the prediction model is to compare the predicted wind field with 15 minutes look-ahead time horizon with the reconstructed field at that time. Fig. 14 shows the contour plots of the wind intensity at Flight Level 350 for these two fields, and it can be seen that the predicted wind field largely agrees with the reconstructed wind field using future data.

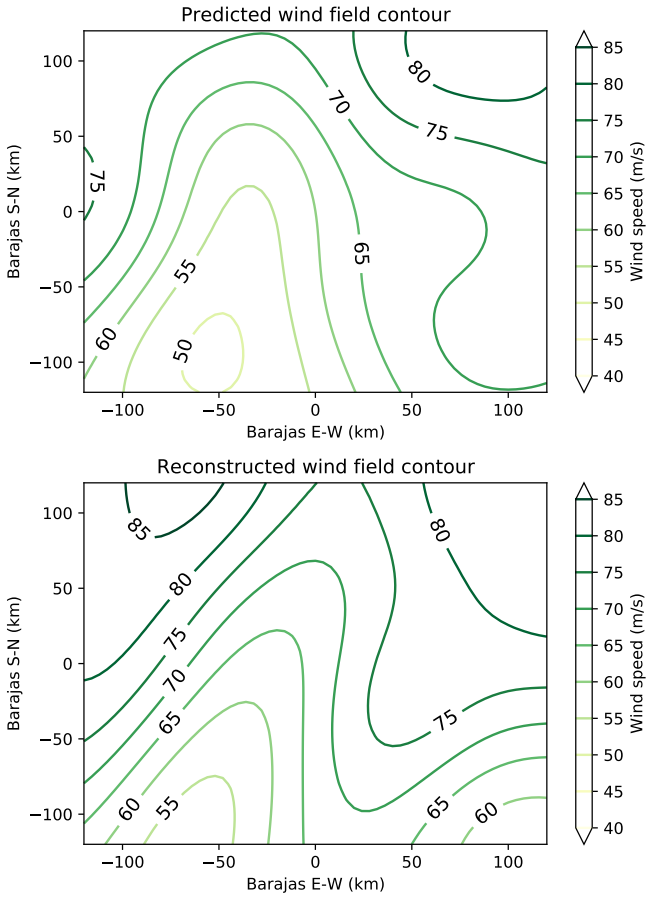

Figure 14. Comparison of predicted and reconstructed wind field at time 14:10 and Flight Level 350.

VII. Conclusion

This paper has explored the applicability of KF and GPR models to generate online and short-term weather predictions from observations derived from ADS-B and Mode S aircraft surveillance data. This approach is possible because the volume, frequency, and coverage of data are high and much larger than those provided by radiosondes or by AMDAR. Furthermore, this technology is already available in the ATM system and data decoders are accessible for open research [7].

At first, the raw information was decoded and wind speed was computed from ADS-B and Mode S ASTERIX data. Then, KF and GPR methods were used to construct wind profile estimations at two relevant positions along the aircraft paths. Thanks to appropriate implementation of the GPR methodology, the GPR model is trained in less than 5 minutes, achieving a large improvement in performance and allowing for nowcasting. All the models have significantly improved the accuracy of the baseline model. Among them, the GPR model has the best performance achieving a RMSE of 3 m/s based on the data we tested. This increased accuracy, reducing to half the baseline model on a windy day, has potential benefits for air traffic performance studies and the future requirements for ATM system, such as updating the optimal descent trajectory in real-time [2] or aircraft spacing [6].

Lastly, the GPR model has been used both to reconstruct and to predict the wind speed field over the TMA. The GPR model can accurately reconstruct the wind field with a low error while generating short-term nowcast. The results are promising and future research is expected on this topic.

In conclusion, this research focused on the development of a theoretical model for accurate wind estimation. On the one hand, selected key locations near the airport were used to demonstrate the capability of the proposed models. On the other hand, the capacity of GPR to estimate wind field has been explored. Future work can be continued to, for example, provide estimations of other meteorological variables such as wind vector or temperature.

ACKNOWLEDGMENT

The authors would like to thank Enrique Gismera Gómez, Ruth Otero Fraguas, and Iciar Sánchez Zorzano from ENAIRE, the Spanish National Air Navigation Service Provider, for providing the data. This work has been partially supported by the grants numbers TRA2017-91203-EXP and RTI2018-098471-B-C33 of the Spanish Government.

REFERENCES

[1] H. Hallot, D. Labyt, and J.-H. Robres, *Meteorology for Aviation*. Cépaduès Editions, 2013.

[2] R. Dalmau, X. Prats, and B. Baxley, "Using broadcast wind observations to update the optimal descent trajectory in real-time," *Journal of Air Transportation*, vol. 28, no. 3, pp. 82–92, 2020.

[3] O. Reitebuch, *The Spaceborne Wind Lidar Mission ADM-Aeolus*. Springer Berlin Heidelberg, 2012, pp. 815–827.

[4] T. G. Reynolds, M. McPartland, T. Teller, and S. Troxel, "Exploring wind information requirements for four dimensional trajectory-based operations," in *Proceedings of the Eleventh USA/Europe Air Traffic Management Research and Development Seminar*, Lisbon, Portugal, June 2015.

[5] S. de Haan, "High-resolution wind and temperature observations from aircraft tracked by Mode-S air traffic control radar," *Journal of Geophysical Research: Atmospheres*, vol. 116, no. D10, 2011.

[6] P. M. A. de Jong, J. J. van der Laan, A. C. in 't Veld, M. M. van Paassen, and M. Mulder, "Wind-profile estimation using airborne sensors," *Journal of Aircraft*, vol. 51, no. 6, pp. 1852–1863, 2014.

[7] J. Sun, H. Vû, J. Ellerbroek, and J. M. Hoekstra, "pyModeS: Decoding Mode-S surveillance data for open air transportation research," *IEEE Transactions on Intelligent Transportation Systems*, vol. 21, no. 7, pp. 2777–2786, 2020.

[8] S. de Haan and A. Stoffelen, "Assimilation of high-resolution mode-s wind and temperature observations in a regional NWP model for nowcasting applications," *Weather and Forecasting*, vol. 27, no. 4, pp. 918–937, 2012.

[9] C. Cardinali, L. Isaksen, and E. Andersson, "Use and impact of automated aircraft data in a global 4DVAR data assimilation system," *Monthly Weather Review*, vol. 131, no. 8, pp. 1865–1877, 2003.

[10] R. Dalmau, M. Pérez-Batlle, and X. Prats, "Estimation and prediction of weather variables from surveillance data using spatio-temporal kriging," in *Proceedings of the 2017 IEEE/AIAA 36th Digital Avionics Systems Conference*, St. Petersburg, FL, USA, September 2017.

[11] J. Sun, H. Vû, J. Ellerbroek, and J. M. Hoekstra, "Weather field reconstruction using aircraft surveillance data and a novel meteo-particle model," *PLOS ONE*, vol. 13, no. 10, pp. 1–33, 2018.

[12] S. Mondoloni, "A multiple-scale model of wind-prediction uncertainty and application to trajectory prediction," in *Proceedings of the 6th AIAA Aviation Technology, Integration, and Operations Conference*, Wichita, Kansas, USA, September 2006.

[13] D. Delahaye, S. Puechmorel, and P. Vacher, "Windfield estimation by radar track Kalman filtering and vector spline extrapolation," in *Proceedings of the* 22^{nd} *Digital Avionics Systems Conference*, Indianapolis, IN, USA, October 2003.

[14] A. M. P. de Leege, M. M. van Paassen, and M. Mulder, "Using automatic dependent surveillance-broadcast for meteorological monitoring," *Journal of Aircraft*, vol. 50, no. 1, pp. 249–261, 2013.

[15] T. Liu, T. Xiong, L. Thomas, and Y. Liang, "ADS-B based wind speed vector inversion algorithm," *IEEE Access*, vol. 8, pp. 150 186–150 198, 2020.

[16] N. Zoumakis and A. G. Kelessis, "Methodology for bulk approximation of the wind profile power-law exponent under stable stratification," *Boundary-Layer Meteorology*, vol. 55, pp. 199–203, 1991.

[17] R. E. Kalman, "A new approach to linear filtering and prediction problems," *Journal of Basic Engineering*, vol. 82, no. 1, pp. 35–45, 1960.

[18] R. Atlas and R. Todling, *Estimation Theory and Foundations of Atmospheric Data Assimilation*. Internal Report of the Data Assimilation Office, Goddard Laboratory for Atmospheres, June 1999.

[19] B. Daya Sagar, Q. Cheng, and F. Agterberg, *Handbook of Mathematical Geosciences*. Springer International Publishing, 2018.

[20] C. Rasmussen and C. Williams, *Gaussian processes for machine learning*. MIT Press, 2006.

[21] L. Bo and C. Sminchisescu, "Greedy block coordinate descent for large scale Gaussian process regression," in *Proceedings of the Twenty-Fourth Conference on Uncertainty in Artificial Intelligence*, Helsinki, Finland, July 2008.